Water Research 156 (2019) 9–22

Contents lists available at ScienceDirect

Water Research

journal homepage: www.elsevier.com/locate/watres

Spatio-temporal dynamics of virus and bacteria removal in dual-media contact-filtration for drinking water

Vegard Nilsen [a, *], Ekaterina Christensen [b], Mette Myrmel [b], Arve Heistad [a]

[a] Norwegian University of Life Sciences, Faculty of Science and Technology, P.O.Box 5003, N-1432, Ås, Norway
[b] Norwegian University of Life Sciences, Faculty of Veterinary Medicine, P.O.Box 8146 Dep, N-0033, Oslo, Norway

ARTICLE INFO

Article history:
Received 20 July 2018
Received in revised form
8 February 2019
Accepted 13 February 2019
Available online 5 March 2019

Keywords:
Drinking water
Filtration
Virus
Dynamics
Modeling

ABSTRACT

Microorganism removal efficiencies in deep bed filters vary with time and depth in the filter bed as the filter collects particles. Improved knowledge of such dynamics is relevant for the design, operation and microbial risk assessment of filtration processes for drinking water treatment. Here we report on a high-resolution spatio-temporal characterization of virus and bacteria removal in a pilot-scale dual-media filter, operated in contact-filtration mode. Microorganisms investigated were bacteriophage *Salmonella* typhimurium 28B (plaque assay, $n = 154$)), fRNA phage MS2 (plaque assay/RT-qPCR, $n = 87$) and *E. coli* (Colilert-18, $n = 73$). Microscopic and macroscopic filtration models were used to investigate and characterize the removal dynamics.

Results show that ripening/breakthrough fronts for turbidity, viruses and *E. coli* migrated in a wave-like manner across the depth of the filter. Virus removal improved continuously throughout the filter cycle and viruses broke through almost simultaneously with turbidity. Ripening for *E. coli* took longer than ripening for turbidity, but the bacteria broke through before turbidity breakthrough. Instantaneous log-removal peaked at 3.2, 3.0 and 4.5 for 28B, MS2 and *E. coli*, respectively. However, true average log-removal during the period of stable effluent turbidity was significantly lower at 2.5, 2.3 and 3.6, respectively. Peak observed filter coefficients λ were higher than predicted by ideal filtration theory. This study demonstrates the importance of carefully designed sampling regimes when characterizing microorganism removal efficiencies of deep bed filters.

1. Introduction

Provision of hygienically safe drinking water is an essential part of public health protection across the world (WHO, 2011). Waterborne microorganisms of concern include pathogenic viruses, bacteria and protozoan parasites, which may reach a point of consumption either by entering raw water sources and overcoming treatment barriers (Mac Kenzie et al., 1994) or by post-treatment introduction into a distribution system (Nygård et al., 2007). Treatment barriers include dedicated disinfection processes as well as general particle separation processes (Hijnen and Medema, 2010). Traditionally, most larger water treatment plants employ some combination of coagulation and deep bed filtration for particle separation.

Viruses may be relatively difficult to remove in particle separation processes (Hijnen and Medema, 2010) and some may be quite resistant to inactivation by disinfection (e.g. Thurston-Enriquez et al., 2003). In fact, enteric viruses have been found in finished drinking water on several occasions (Keswick et al., 1984; Rose et al., 1986; Payment and Armon, 1989). Therefore, in a multiple-barrier approach to microbial water quality, operational optimization and sound estimates of virus removal efficiencies of each unit process are needed. Virus removal during depth filtration, and its relationship to effluent turbidity, was recently identified as a knowledge gap in microbial risk assessment (Petterson and Ashbolt, 2016), and virus removal is the main focus of the research reported in the present paper.

Since typical Norwegian surface waters are low in turbidity but high in natural organic matter (NOM), most plants are designed as direct filtration or contact filtration plants (Ødegaard et al., 1999, 2010), i.e. filtration without a preceding sedimentation step. A coagulation-filtration system that meets specific regulatory requirements, mainly with respect to effluent turbidity, color and residual coagulant content, is recognized as a *hygienic barrier* in

* Corresponding author.
E-mail address: vegard.nilsen@nmbu.no (V. Nilsen).

https://doi.org/10.1016/j.watres.2019.02.029

Norwegian regulations and assumed to be capable of removing viruses, bacteria and parasites by 3, 3 and 2 $\log_{10}$-units, respectively. However, other guidelines issued by the Norwegian water industry association (Ødegaard et al., 2014), partly modeled on the USEPA Surface Water Treatment Rule (USEPA, 2006), only credit direct filtration systems with a log-removal capacity for viruses of 1.5 if effluent turbidity is $<$ 0.2 NTU, or 2 if enhanced coagulation is used with effluent turbidity $<$ 0.1 NTU and color removal better than 70%. A recent report (Eikebrokk, 2012) in Norway recommended that the virus removal efficiency of contact-filtration processes in particular be investigated in greater detail.

The deep bed filtration process is inherently dynamic, even if the influent water quality is stable: filter performance varies with time and with depth in the filter bed as the filter collects particles (Adin and Rebhun, 1974; Tien and Ramaro, 2007). Although there is usually a prolonged period of stable effluent turbidity after ripening and before breakthrough, the removal efficiency for individual particle types, such as microorganisms, may be more dynamic than turbidity removal (e.g. Clark et al. (1992)). Characterizing these variations is important for determining optimal filter operation to minimize pathogen passage (Huck et al., 2001). The filtration process is also periodic and discontinuous since regular backwashing is required to restore the particle removal capacity. Hence, average removal efficiencies during filtration may be challenging to estimate or, at worst, insufficient for characterizing health risks since the temporal variation in pathogen concentrations may be needed for a proper quantitative microbial risk assessment (QMRA; Haas et al., 2014).

The dynamic characteristics of the process imply that frequent sampling is needed in order to capture the full variation and allow true average removal efficiencies to be computed.[1] However, high-resolution spatio-temporal characterization of virus removal efficiency in deep bed filters has hardly been undertaken, with most studies relying only on samples from the filter outlet at relatively coarse time intervals. Presumably, this is partly due to the cost and labor-intensive experiments that are needed for a detailed characterization. Obtaining more complete characterizations of the virus removal efficiency could lead to a better understanding of the virus removal dynamics, which could subsequently inform QMRA studies and decisions on the design and operation of deep bed filters.

Tables S.1 and S.2 in the online supplementary material provide a summary of 25 previous studies on virus removal in deep bed filtration for drinking water where coagulation was employed at some point upstream of the filter. In general, adequate particle stabilization by coagulation is necessary for effective rapid filtration (Amirtharajah, 1988) and very poor virus removal is observed in rapid deep-bed filters if coagulation is not employed (see e.g. Huck et al. (2001); Hendricks et al. (2006)). The results in Tables S.1 and S.2 vary significantly, from almost no removal to more than 5 log-removal. While it is difficult to pinpoint the exact reasons for this variation in each case, differences between virus species certainly may play a role, and it is obvious that the operational conditions under which the results were obtained also varied significantly. There seems to be a trend (Tables S.1 and S.2; Hijnen and Medema (2010)) that removal efficiencies obtained from full-scale studies are lower than those observed at pilot or bench scale. Workers who compared different filter configurations (depth, media, filtration rates) under otherwise similar conditions found only moderate differences in removal. Some workers investigated removal during ripening and/or breakthrough periods and found prolonged ripening for viruses compared to turbidity (Robeck et al., 1962) and reduced removal during these periods (Templeton et al., 2007). Templeton et al. (2007) also suggested that the degree of virus-particle-association, relevant for downstream disinfection processes, may vary during a filter cycle. With the exception of Templeton et al. (2007), who sampled mid-cycle from the interface between anthracite and sand media, none of the 25 studies sampled from multiple levels of the filter column.

The purpose of the present study was therefore to undertake a detailed, high-resolution experimental investigation of a pilot-scale dual-media contact-filtration system with respect to virus removal throughout the entire filter column and the whole filtration cycle. A tailor-made automatic sampler was constructed to facilitate controlled, consistent and simultaneous sampling from eight levels of the filtration column without significantly disturbing the system hydraulics and thereby filtration behavior. Two model bacteriophages, *Salmonella* typhimurium 28B and f-specific bacteriophage MS2 were used, while *E. coli* was also included as a bacterial reference. Measures were taken to characterize potential aggregation effects and account for known virucidal/inhibitory effects of the polyaluminium-chloride coagulant (Kreiβel et al., 2014; Willumsen, 2015), which otherwise may affect results significantly. A sub-goal of the project was to produce data that are suitable for fitting a dynamic filtration model through inverse modeling; this work is ongoing. A small subset of the data has already been published in a paper that compared the mid-cycle removal efficiencies when using different coagulants (Christensen et al., 2017).

2. Materials and experimental methods

2.1. Pilot-plant design

An overview of the pilot-plant is given in Fig. 1. The filter column was made from a transparent PVC cylinder with 10 cm inner diameter. A 10 cm deep support layer with size graded gravel covered the outlet, a tapered plastic cone with slits. The bottom filter medium consisted of 50 cm of 0.4–0.8 mm silica sand (Rådasand AB, Sweden). The top filter medium consisted of 79 cm of 0.8–1.6 mm expanded clay aggregates (Filtralite NC - normal density, crushed; Weber Saint-Gobain, Norway). Filtralite has been shown to produce similar filtrate quality as anthracite, but with slightly slower headloss development (Eikebrokk and Saltnes, 2001). The physical characteristics of the filter media, as specified by the manufacturers, are given in Table 1. The ratio of column diameter to effective grain size was greater than 50, the recommended minimum ratio to minimize wall effects (Mehta and Hawley, 1969; Lang et al., 1993).

Raw water was stored in a 30 m^3 underground tank equipped with a circulation pump. Prior to a filter run, a batch of raw water was pumped from the underground tank into a smaller steel tank (1.8 m^3, with a paddle stirrer) in the laboratory. Water was fed from the steel tank at a constant rate by feed pump P1 (Watson Marlow 620U hose pump with 620RE4 pump head and LoadSure 12 mm tubing) and entered the column through a pipe that was submerged except during the very early stages of the filter cycle. The hydraulic head on the effluent side of the column was kept constant by a container with an overflow; thus the filter was operated in constant rate, rising head mode. Tap water was used for backwashing, with the flow rate controlled manually with a tap.

The microorganism suspension, hydrochloric acid (HCl, for pH adjustment) and polyaluminium chloride (PACl) coagulant (PAX-18, Kemira AS) were added to the 19 mm diameter main supply tube in tee fittings using peristaltic dosing pumps (Watson Marlow 120U/DV with 114DV pump head) P2, P3 and P4, respectively. The inline

[1] Mean removal may also be obtained through continuous flow-proportional sampling, but this provides no information on temporal variation in removal efficiency.

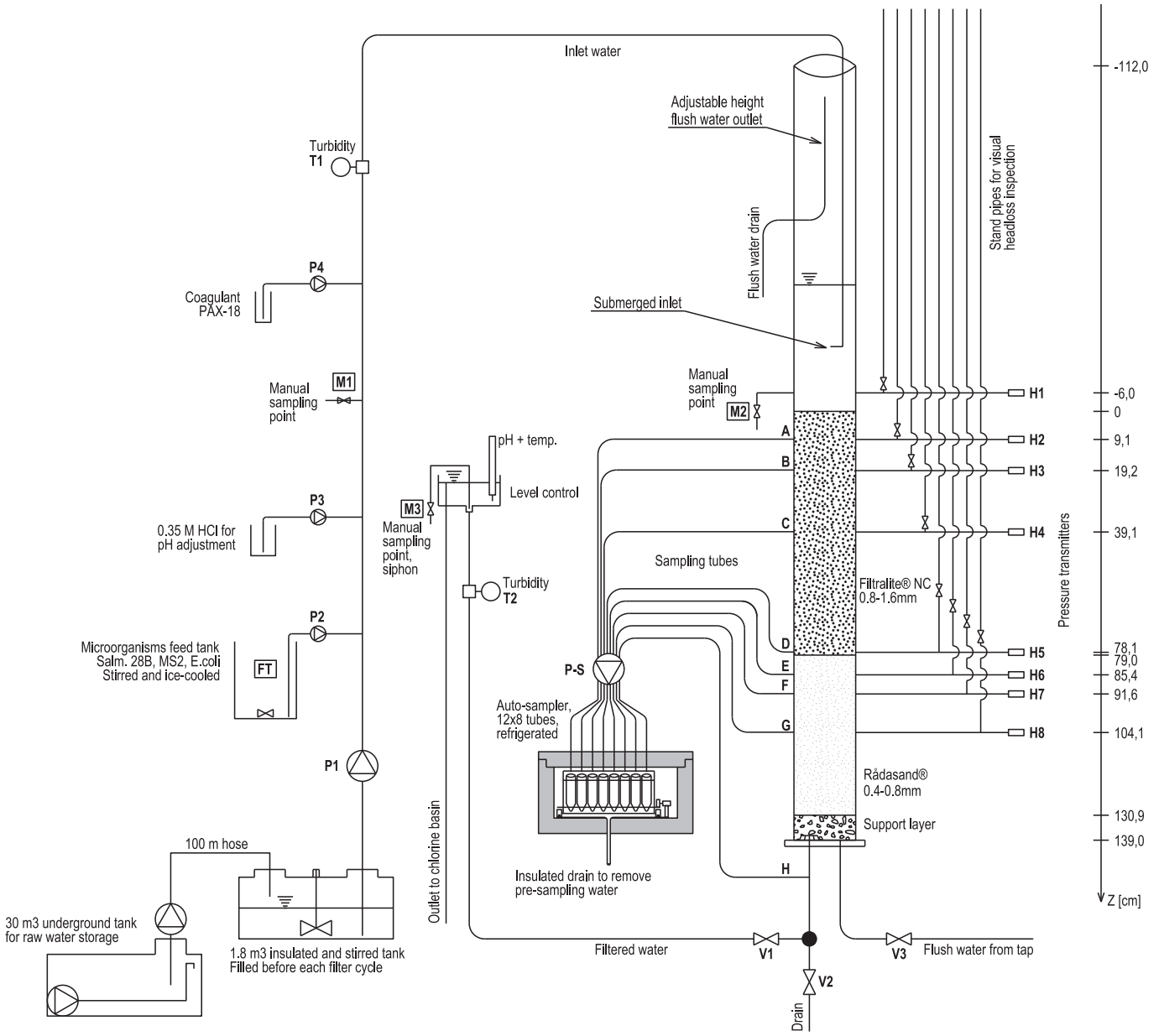

Fig. 1. Schematic overview of the pilot-scale filtration plant. Manual sampling points are labeled with text boxes.

Table 1
Filter material physical data, as reported in the respective manufacturers' data sheets (available in the online supplementary material).

Parameter	Filtralite	Rådasand
Layer depth (m)	0.79	0.5
Grain size, nominal range (mm)	0.8–1.6	0.4–0.8
Effective grain size, d_{10} (mm)	0.95	0.4
Column diameter/d_{10} (–)	105	250
Uniformity coefficient, d_{60}/d_{10} (–)	<1.5	<1.8
Primary porosity (–)	0.58	0.45
Bulk porosity (–)	0.80	0.45
Grain density (kg/m^3)	1260	2600
Bulk density (kg/m^3)	530	1440

Table 2
Primers and probe sequences for MS2 RT-qPCR analyses. Taken from Dreier et al. (2005) with some modifications in primers/probe volumes.

Primers and probe	Sequence (5′-3′)
MS2-TM2-F (400 nM)	TGCTCGCGGATACCCG
MS2-TM2-R (400 nM)	AACTTGCGTTCTCGAGCGAT
MS2-TM2FAM (50 nM)	FAM-ACCTCGGGTTTCCGTCTTGCTCGT-BHQ1

part of the tees consisted of a 7 cm long 6 mm diameter pipe section with a sudden contraction and expansion, generating turbulence at the exit for rapid mixing of chemicals/microorganisms. Effective mixing was observed when testing the mixer using a dye. Online turbidimeters (WTW Visoturb 700 IQ) were installed on both the influent and effluent sides of the column, and calibrated for in-pipe-installation according to the manufacturer's instructions. An online pH-meter and temperature sensor (WTW SensoLyt 700 IQ) was installed on the effluent side in the overflow container. Eight online pressure transmitters H1-H8 (Impress IMP-LR 250 mbar) were installed with non-uniform spacing in order to focus data

collection from the portions of the filter where the largest hydraulic gradients were expected to occur. Hydraulic head could also be visually inspected in eight standpipes. A LabView application (National Instruments, USA), communicating with sensors/valves/pumps through a micro-controller, was used for control, monitoring and logging of recorded data.

Ports for automated water sampling (A-H) were installed directly opposite the ports for pressure monitoring (A-G) and in the column outlet (H). Ports A-G contained a cylinder protruding about 15 mm into the filter media in order to minimize the influence of wall effects during sampling. The automatic sampler consisted of an 8-channel peristaltic pump (Ismatec ISM843A) that directed samples into a refrigerated (approximately 4 °C), insulated box. The box contained a moving tube rack, controlled by an optical sensor and electrical motor, for sample collection and storage. Sampling tubes were cut to equal length and prior to each sampling event, a volume corresponding to three full tube lengths would be drained to waste before actual sampling commenced. This ensured that water in the tube from the previous sampling event was replaced by fresh water from the current sampling event. The insulated box could take 12 sets of samples, each consisting of eight 50 ml centrifuge tubes, i.e. 96 samples.

In addition to the automated samples, manual samples could be taken from locations M1 and M2 (before and after addition of coagulant, for assessment of possible aggregation and virucidal/inhibitory effects of the coagulant) as well as from the outlet M3. Manual samples could be taken more frequently than the automatic samples and allowed better monitoring of the ripening and breakthrough periods. Samples could also be taken from the microorganism feed tank (FT).

2.2. Microorganisms

2.2.1. Salmonella typhimurium 28B

Salmonella typhimurium phage 28B (Lilleengen, 1948) is a double-stranded DNA bacteriophage. It has a head (50 nm) with an octagonal outline which is attached to a smaller structure (a baseplate) that extends approximately 10 nm from the head (Svenson et al., 1979). The phage does not occur naturally in the environment and has been shown to be heat resistant (Sahlström et al., 2008). In our experience, stock suspensions can be kept for years at refrigeration temperatures without significantly loosing the titer. Phage 28B was included in this study for its relatively simple and robust propagation and enumeration protocol.

The phage was propagated and enumerated according to an unpublished protocol from the Public Health Agency of Sweden, but essentially as described by Höglund et al. (2002) and equivalent to ISO 10705–2 (ISO, 1999), using its bacterial host strain *Salmonella enterica* subsp. *enterica* Typhimurium type 5. The growth medium consisted of distilled water with nutrient broth (0.8% w/v; 105443, Merck, Germany) and yeast extract (0.05% w/v; 111926, Merck, Germany).

For phage 28B propagation, 0.25 ml of overnight bacterial host culture was transferred into 25 ml of fresh growth medium and incubated for 2 h at 37°C shaken. A volume of stock 28B phage suspension was added to achieve a ratio of phage to host concentrations of 1:200, using known stock phage concentrations and an assumed host culture concentration of $2 \cdot 10^8$ cells/ml (from the unpublished protocol). This mixture of phage and host was incubated shaken at 37°C for 10–12 min before diluting with 500 ml fresh growth medium. The diluted suspension was incubated at 37°C shaken for 4–5 h. After incubation, 10 ml/l of chloroform was added to kill and lyse the host cells. The suspension was then centrifuged for 10 min at 3000 rpm and filtered through a 0.45 μm filter. The final concentration was determined to be $5 \cdot 10^9$ PFU/ml (plaque forming units/ml).

Phage 28B enumeration was performed as a double-layer agar plaque assay, similar to ISO 10705–2 (ISO, 1999). Fresh bacterial host cultures were prepared by inoculating 25 ml of growth medium with 0.25 ml of existing host culture and incubating at 37°C shaken for 4 h. Host cultures were used for enumeration between 4 and 8 h after inoculation. Petri dishes with 20 ml solid bottom-agar (growth medium with 1.5% w/v agar) were prepared. Four ml molten top-agar (growth medium with 0.65% w/v agar kept at about 50°C) was mixed with 0.5 ml sample (after serial dilution in 0.9% NaCl, when required) and 0.5 ml exponential-phase bacterial host culture and poured over the solid agar. Samples were incubated at 37°C for approximately 18 h and plaques were counted.

Preliminary investigations (Willumsen, 2015) revealed that titres of phage 28B sampled from point M1 (before coagulant addition) remained stable during a few days of storage while titres sampled samples from M2 and M3 (after coagulant addition) steadily decreased by up to 1.5–2 $\log_{10}$-units during one week (Figures S.3 and S.4 in the online supplementary material demonstrate this effect). Thus, a slow virucidal and/or aggregation effect of the coagulant appears to be present. In order to reduce the impact of this effect, all samples were analyzed promptly after sampling (plated within 1–4 h for all samples). Not all dilutions could be plated in replicates (due to the intense sampling regime), but at least two plates were incubated for every sample (two dilutions and/or parallels of the same dilution). Figure S.6 in the online supplementary material shows uncertainty estimates for each sample.

2.2.2. MS2

F-specific bacteriophage MS2 is a 27 nm icosahedral single-stranded RNA virus (Strauss Jr. and Sinsheimer, 1963). It was included in this study since it is commonly used as a surrogate for pathogenic viruses when assessing the performance of water treatment processes (as seen in Tables S.1 and S.2 in the online supplementary material). It was propagated according to ISO 10705–1 (ISO, 1995) against the host *Salmonella* Typhimurium WG49 (NCTC 12484). Most MS2 enumerations were performed using reverse transcription quantitative polymerase chain reaction (RT-qPCR), but a few samples were also enumerated using a plaque assay in order to assess the absolute number of viable MS2 viruses present and to provide a rough comparison of log-removal values obtained from qPCR data.

Previous studies (Matsui et al., 2003; Matsushita et al., 2011; Kreißel et al., 2014), as well as preliminary investigations for this study, have shown that PACl coagulants tend to lower the concentrations of f-specific phages like MS2, even at low doses, as measured by a reduced infectivity in plaque assays. Kreißel et al. (2014) attributed the effect to interaction between MS2-surfaces and dissolved polymeric aluminum species Al_{13}, speculating that it prevents the phage-host binding necessary for successful infection. In order to decrease the impact of this effect in the present study, the method of Matsushita et al. (2004) was performed prior to plaque assay. A solution of beef extract (BE) was prepared with 13% BE powder (211520, Becton, Dickinson and Company, USA) and 5 N NaOH was added to reach a target pH of 9.5–10.0. The BE solution was kept at 4 °C and used within three days. All MS2 samples were diluted 10-fold with BE and then stirred at 1500 rpm at 4 °C for at least 5 h. The plaque assay for MS2 was then performed on the treated samples as described by Debartolomeis and Cabelli (1991), using *Escherichia coli* Famp as the host. The method has also been evaluated for water samples without PACl coagulants and it then usually shows 0.2–0.3 $\log_{10}$ units higher titres compared to untreated samples (Christensen and Myrmel, 2018).

For RT-qPCR, viral RNA was extracted from 140 μl water samples

with the QIAamp Viral RNA Mini kit and QIAcube automated purification system according to the manufacturer's (Qiagen, Germany) instructions with minor modifications: the samples were stored in 560 μl lysis buffer at − 80°C and were spiked after thawing with carrier-RNA (3.1 μg per sample) prior to RNA-extraction. RT-qPCR was done with a Stratagene AriaMx Real-Time PCR System (Agilent Technologies, USA). An aliquot of 3 μl of the RNA was added to 17 μl of the reaction mixture (UltraSense One-Step Quantitative RT-PCR System kit, Invitrogen, USA) containing 4 μl 5x Reaction Mix with 0.2 nM of each dNTP, 1 μl Enzyme Mix, 0.4 μl of ROX dye, 400 nM of forward primer, 400 nM of reverse primer and 50 nM of probe. Primers and probe sequences are listed in Table 2. The temperature sequence was 30 min at 55 °C, 2 min at 95 °C, 45 cycles of 15 s at 95 °C and 30 s at 58 °C. Each sample was run in duplicate. ROX was used as a passive fluorescence reference and positive and negative (no template) controls were included on all plates. Aliquoted homologous RNA was also included on each plate as an inter-plate calibrator (IPC).

Baseline correction was performed automatically by the Agilent AriaMx 1.1 Software (Agilent Technologies, USA). Interplate calibration (Hellemans et al., 2007) was performed by setting the threshold for each plate individually so as to make the mean C_q-values (quantification cycles) for the IPCs equal, while ensuring that all thresholds were in the exponential region of the amplification curves. One of the plates included a 10-fold serial dilution series of homologous viral RNA, run in triplicate, for determination of the amplification efficiency E ($E = 88.7\%; R^2 = 99.8\%$), which was assumed to be equal among plates. Under these conditions, the ratio of concentrations c_2/c_1 in any two samples (same or different plates), indexed by 1 and 2, is given by the qPCR equation (details in the online supplementary material)

$$\frac{c_2}{c_1} = (1+E)^{C_{q,1}-C_{q,2}} \quad (1)$$

The absolute amount of RNA used for the IPCs and the serial dilution was not known, but nor is it needed for calculating the ratios in (1). These ratios are all one needs to compute removal efficiencies as presented in Section 3. Figure S.7 in the online supplementary material shows uncertainty estimates for each sample.

Preliminary experiments were performed to test for potential interference effects of the coagulant with the PCR assay. Distilled water was spiked with MS2 and coagulant and underwent RNA extraction and RT-qPCR analysis as described above. No interference effects were observed for coagulant concentrations up to 10 mg/l when compared with control samples without coagulant.

2.2.3. Escherichia coli

E. coli was also included in this study for comparison with the viruses and because it is a widely used faecal indicator bacterium (Edberg et al., 2000). Cultures were prepared by inoculating brain-heart infusion broth (237500, Becton, Dickinson and Company, USA) with *E. coli* (CCUG 17620). Overnight cultures were centrifuged and washed twice with peptone saline diluent (CM0733, Oxoid, United Kingdom) and stored at 4 °C for a maximum of 5 days. Enumeration of *E.coli* was performed using Colilert-18 with Quanti-Tray/2000 (IDEXX Laboratories, USA) according to the manufacturer's instructions. The method is equivalent to a most probable number (MPN) method with two dilutions and 48/49 tubes at each dilution. Samples were analyzed using only one replicate due to time constraints. Figure S.8 in the online supplementary material shows uncertainty estimates for each sample.

2.3. Water quality analyses

Manual turbidity measurements, including the samples from port A-H, were performed with a HACH 2100N IS benchtop turbidimeter according to the manufacturer's instructions. Due to time constraints, most of these turbidity measurements had to be performed during the days following the experiment and were subject to changes due to storage. For the effluent both continuously logged turbidity (sensor T2 in Fig. 1) and manually measured turbidity (samples from port H) was available. The difference in turbidity between samples from port H and logged values from sensor T2 was on average 0.055 (SD: 0.020) units. Assuming that this increase due to storage is relevant for all the manual turbidity measurements, 0.055 NTU was subtracted from all the manual measurements for ports A-H as a crude way of accounting for changes due to storage.

Color and UV-absorption measurements were done on spectrophotometer HACH DR 3900 after filtering the samples through a 0.45 μm filter. Raw water alkalinity was determined by titration with HCl to pH 4.5, using the dosing pump and pH meter in the pilot plant. Raw water total organic carbon (TOC) was measured by an external lab (ALS Laboratory Group AS, Norway) according to NS-EN 1484:1997. The suspended solids content of the coagulated water was measured according to method NS-EN 872:2005. Total residual aluminium concentration was determined during a test run using HACH Aluminon method 8012, adapted from Standard Methods no. 3500-Al (APHA/AWWA/WEF, 2012). During the actual experiment, dissolved aluminium was determined by an external lab (Noranalyse AS, Norway) using ICP-OES according to method NS-EN ISO 11885:2009. All measurements mentioned in this paragraph were taken immediately after sampling except for suspended solids and the external lab analyses (TOC and one Al-analysis), which were done a few days after the experiment.

2.4. Raw water quality and coagulant dose determination

The raw water was collected from the river Glomma on two occasions (August 2014 and May 2015) and mixed in the storage tank at the university. After some initial sedimentation, turbidity remained stable in the storage tank. As explained in Section 2.1, a batch of raw water would be pumped into the lab prior to each filter run. The measured raw water characteristics of the experimental batch are listed in Table 3. Figure S.5 in the online supplementary material shows raw water quality time series taken during the experiment. The specific UV-absorption (SUVA) is relatively high,

Table 3
Raw water characteristics and operational conditions during the experiment. For raw water, the intervals indicate the range in measured values over time. No intervals given indicate only a single measurement was taken. The standard deviation for TOC is for two replicates of a single sample.

Parameter	Value
Raw water turbidity (NTU)	0.7–0.8
Raw water color (mg Pt/l)	24–27
Raw water TOC (mg/l)	3.03 ± 0.61
Raw water UV absorption (1/m)	13.1
Raw water SUVA[a] (l/(m·mg))	>4.3
Raw water pH (−)	7.3–7.35
Raw water alkalinity (mM)	0.28
Raw water temp. (°C)	15–16
Filtration rate (m/h)	5.9
Flow rate (l/min)	0.77
PAX-18 dose (mg Al/l)	1.5
HCl dose (mM)	0.12
Initial total headloss (cm)	26

[a] Specific UV absorption (UV absorption/DOC).

indicating that the NOM of this water is rich in aromatic compounds and well suited to treatment by coagulation (Matilainen et al., 2010).

PAX-18 (Kemira, Finland), a 42% basicity polyaluminium chloride with an Al-content of 9% (w/v), was chosen as the coagulant for this study as it is a commonly used coagulant in Norway. No filter aid was used. HCl was used for pH-adjustment prior to adding the coagulant. The filtration rate was kept constant at 5.9 m/h. The coagulant dose and coagulation-pH were determined by testing a range of doses and pH-values in the pilot plant, searching for the smallest dose (and the best-working pH at that dose) that resulted in outlet turbidity values less than 0.2 NTU, color less than 5 mg Pt/l and residual coagulant content < 0.15 mg Al/l, which are the main Norwegian regulatory requirements for an Al-based coagulation-filtration plant to be considered a hygienic barrier.

It was found that a coagulant dose of 1.5 mg Al/l and coagulation-pH of 5.8 constituted an optimal dosing regime, resulting in effluent turbidity of 0.03–0.04 NTU, color <2 mg Pt/l and residual aluminium concentration of 0.031 mg Al/l during the optimization run. Subsequently, a full filtration cycle with this dose showed that the cycle was terminated by turbidity breakthrough after approximately 15 h. The dose and the filter run length are in rough agreement with empirical models developed by Eikebrokk et al. (2004) based on numerous pilot filter runs with low-turbidity waters and a range of color values.

It should be noted that no microorganism suspension was added to the influent water during dose optimization. Thus, the particle content and water chemistry may have changed during the actual experiment, but no significant changes in the process could be observed. Specifically, the effluent turbidity evolution during the experiment was close to that observed during the trial run described in the previous paragraph. Approximate net dilution factors for the addition of stock microorganism suspensions to the influent water were 1:26000 (28B), 1:6500 (MS2) and 1:11000 (*E. coli*).

2.5. Experimental protocol

Prior to a filter run, the column was backwashed for approximately 15 min at a rate of 50–60 m/h, resulting in a filter expansion of 50–60%. The backwash rate was reduced gradually towards the end of the backwash in order to promote good separation of the two media, but some interfacial mixing was still observed. The system was then run with raw water for approximately 15 min in order to displace the tap water present in the filter from backwashing. This was considered to give a more realistic initial condition since the tap water came from a different raw water source than the one used for the experiment, and may also have contained some residual chlorine. After 15 min of running raw water, dosing of microorganisms, HCl and coagulant was initiated simultaneously.

Time, cost and raw-water availability meant that only a single filter-run with high-resolution sampling could be performed. An overview of the sampling regime employed for this study is given in Table S.4 in the online supplementary material. Samples were taken uniformly spaced in time except for samples from point M3, which were taken more frequently during the ripening and breakthrough periods. A total of 160 water samples were taken during the filter cycle, of which 154 were analyzed for 28B, 9 by plaque assay for MS2, 78 by RT-qPCR for MS2, 73 for *E. coli*, 119 for turbidity, 9 for color and 1 for aluminum, giving a total of 443 data points.

The automatic sampler was programmed to take samples with a total flow rate of 40 ml/min (~5% of the total flow rate through the column), i.e. 5 ml/min per sampling port (~0.625% of the total flow rate). This ensured that the water velocities through the sampling ports were lower than the pore water velocity, reducing the risk of eroding the deposit by sampling-induced shear forces. The sample collection duration was 10 min in order to fill up the 50 ml centrifuge tubes in the automatic sampler, and concentrations calculated from these samples should therefore be interpreted as 10 min averages. As described in Section 2.1, prior to each sampling event the sampler would drain the sampling tubes to replace water from the previous sampling event with fresh water from the column. The draining would also last 10 min, replacing the water in the tubes approximately three times, using the same flow rate as during sampling.

The possibility of virus adsorption in the sampling tubes of the automatic sampler was assessed by pumping coagulated water containing viruses through one of the tubes, and enumerating phage 28B before and after tube passage. A reduction in phage concentration of 7% was observed (although not statistically significant at the 95% level; $p = 0.27$) and considered acceptable. Section S.5 in the online supplementary material gives details on this statistical analysis.

2.6. Data presentation

Time points for all samples collected outside of the filter column (online turbidity, pH, temp., M1, M2 and M3) have been adjusted for the flow time in tubes/pipes, assuming plug-flow. Time points for the automatic samples have been set to the midpoint of the 10-min sampling duration. Time zero corresponds to initial arrival of the coagulated water at the filter surface.

3. Experimental results with discussion

3.1. Water quality

Water quality results are shown in Table 4 and temporal variation, where available, is given in Figure S.5 in the online supplementary material. Effluent pH decreased initially to reach a stable value of 5.9–6.0 after 2–3 h; this initial decrease we suspect is due to a slightly pH-raising effect of the top Filtralite medium which subsides when the medium is covered with deposit. Fig. 2 shows that online effluent turbidity reached a stable level after approximately 3 h and breakthrough started at approximately 14.2 h. Online inlet turbidity (Fig. 2d, "IN") showed an increasing trend which we attribute to particles accumulating in the vertical pipe in which the sensor was installed (the upwards flow velocity of ~0.5 cm/s was probably close to the terminal velocity of some of the influent particles). True influent turbidity likely remained stable around the initial value of ca. 2.05 NTU.

Table 4
Water quality results and influent microorganism concentrations. Temporal variation in water quality, where available, is shown in Figure S.5 in the online supplementary material.

Parameter	Value
Influent turbidity (NTU)	~2.05
Influent SS (mean ± SD (replicates); mg/l)	8.2 ± 0.42
Influent coagulation pH (–)	5.8
Effluent pH (–)	5.9–6.0
Effluent color (mg Pt/l)	3
Effluent residual Al-content (mg Al/l)	0.031[a]/<0.010[b]
Influent 28B conc. (mean ± SD; PFU/ml)	$2.57 \pm 0.55 \cdot 10^5$
Influent MS2 conc. (mean ± SD; PFU/ml)	$1.96 \pm 0.31 \cdot 10^6$
Influent *E. coli* conc. (mean ± SD; MPN/100 ml)	$9.31 \pm 2.5 \cdot 10^5$

[a] During dose optimization, total (HACH method).
[b] During experiment, dissolved (external lab).

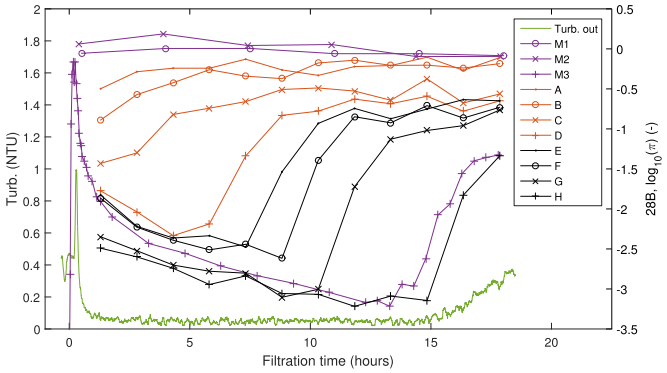

(a) Phage 28B concentrations normalized to influent concentrations.

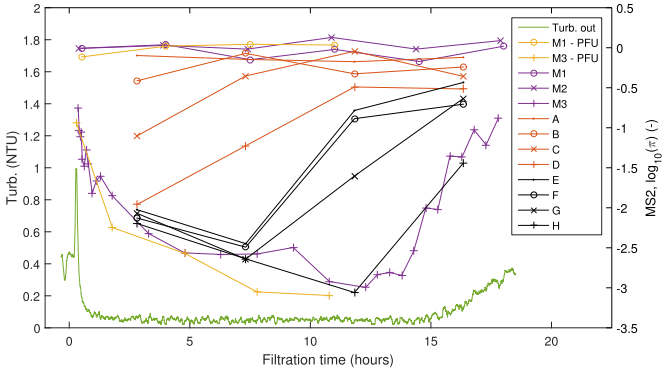

(b) Phage MS2 concentrations normalized to influent concentrations. All datapoints stem from RT-qPCR analyses except for the yellow lines/points which stem from the plaque assay.

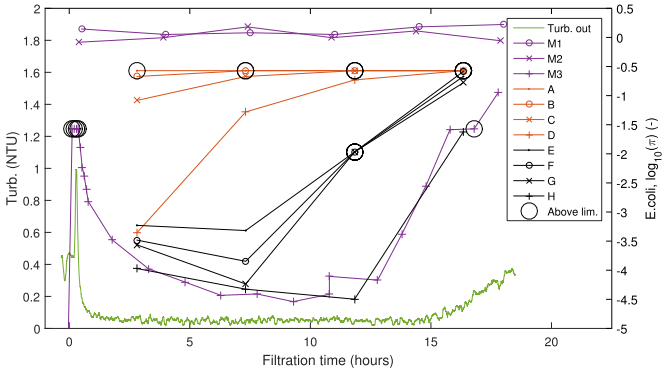

(c) *E. coli* concentrations normalized to influent concentrations. Note that several A-G samples were above enumeration limits (labeled) and the data should be interpreted with care.

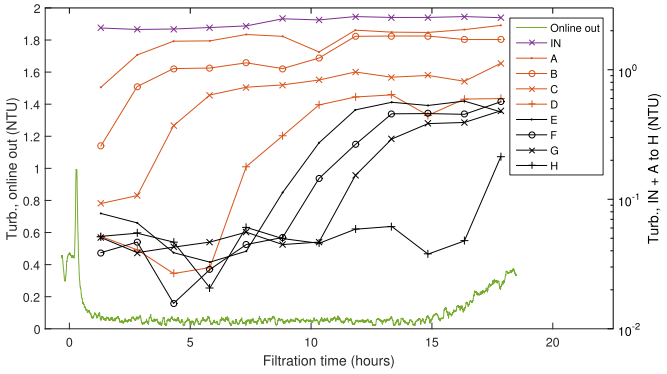

(d) Turbidity, online and manual measurements.

Fig. 2. Spatio-temporal passage of microorganisms and turbidity.

3.2. Spatio-temporal removal

No major differences in microorganism concentrations were found between sampling ports M1 before coagulant dosing and port M2 after coagulant dosing (see Fig. 2, introduced below), suggesting that neither microorganism aggregation nor inhibition effects from the coagulant were present to any appreciable extent between coagulant dosing and sample analysis. Mean influent concentrations c_{in} of each organism were calculated from all M1 and M2 samples and are given in Table 4. These were used to compute the passage probability $\pi = c/c_{in}$ for all sample ports, where c is the concentration in the sample port. The log-removal is simply $-\log_{10}(\pi)$. Fig. 2 shows the results of all spatio-temporal sampling for phage 28B (2a), phage MS2 (2b), *E. coli* (2c) and turbidity (2d). Microorganism removal in Fig. 2 is presented in terms of $\log_{10}(\pi)$. For visual clarity, uncertainty estimates are not included in Fig. 2; these are instead shown in Figures S.6 - S.8 in the online supplementary material. In general, looking at the steepness of the curves, Fig. 2 confirms that the 10 min sample collection time in the automatic sampler was relatively short compared to the time needed for changes in the local concentrations to occur, i.e. the time-averaging effect behind each datapoint is relatively small.

3.2.1. Salm. typh. 28B

Fig. 2a clearly shows the existence of ripening and breakthrough fronts that migrated across the depth of the filter as the cycle progressed. Overall removal continued to improve until breakthrough of 28B after approximately 13 h, slightly before turbidity breakthrough. Log-removal remained higher than 2.5 for most of the cycle and peaked at about 3.2. It can be seen that at the time of the first auto-sample, breakthrough of 28B had already occurred at ports A, B and C while the lower parts of the filter were still in a ripening phase. Fig. 2a shows that after breakthrough in a given port, the concentrations in that port increased before reaching a plateau. At the end of the cycle there was still some removal occurring (~1.3 $\log_{10}$ units), mainly between ports B and C (~0.4 $\log_{10}$ units), and between port G and the outlet (~0.5 $\log_{10}$ units).

Sampling from multiple depths effectively allows a study of the impact of media configuration and filter depths in a single filter run. The peak log-removal in the upper layer (Filtralite, as measured by port D) was around 2.3, compared to the overall peak of 3.2. This is in agreement with previous research that found moderate effects of filter depths and media configurations on virus removal (Hijnen and Medema, 2010; Harrington et al., 2003; Hendricks et al., 2006). This may be explained by the fact that only a relatively small part of the filter is responsible for the majority of the removal at any given time, since ripening occurs progressively across the depth of the filter. However, breakthrough in the Filtralite medium occurred already after approximately 4 h. Thus, while filter depth and media configurations may have a moderate effect on *peak* removal efficiencies, a deeper filter may extend the useful operating period and decrease the number of breakthrough and initial ripening periods per unit time, thereby improving the overall *mean* log-removal.

There are some inconsistent results in Fig. 2a. Early in the cycle, there is some removal between ports F and G, but not between ports D and F which is inconsistent with the assertion that ripening occurs progressively with depth. Also the concentrations in the manual samples from the outlet (M3) are above those from ports G and H early in the cycle. We do not have a firm explanation for these results, although the early G and H concentrations may have been underestimated because of high plaque counts on some Petri dishes. In general, we trust the manual sampling data somewhat more than the auto-sampler data.

3.2.2. MS2

The sampling frequency for MS2 is lower than for 28B, but the results for the auto-samples are qualitatively similar (Fig. 2b). Compared to 28B, removal was slightly poorer for MS2 analyzed by RT-qPCR (more clearly seen in Fig. 3, introduced below) and peaked at about 3 $\log_{10}$-units after 12–13 h. Data from plaque assays and RT-qPCR are largely consistent, with plaque assays apparently indicating a slightly better removal. If this is really so, it could be caused by some residual inhibitory effect of the coagulant even after the BE treatment, or possibly some non-infectious PCR-units that are more poorly removed than infectious MS2. However, there is a mid-cycle rise in outlet concentrations from RT-qPCR that was not observed for the plaque assay or any of the other organisms. While the data does not allow firm interpretations, we may speculate that this could be related to a breakthrough in the upper part of the filter before sufficient ripening for MS2 has occurred in the lower parts of the filter.

3.2.3. E. coli

The sampling frequency for *E. coli* is also coarser than for 28B, but ripening and breakthrough fronts can be observed here as well (Fig. 2c). Note that all A-samples and several B- to G-samples were above the enumeration limit for the Colilert-18 method; hence $\log_{10}(\pi)$ is closer to zero for these samples than shown in Fig. 2c. Removal peaked at about 4.5 $\log_{10}$-units, but this occurred mid-cycle after approximately 9 h and *E. coli* removal had deteriorated significantly by the time of turbidity breakthrough.

3.2.4. Turbidity

The turbidity data (Fig. 2d) from within the filter column displays a pattern similar to that of the 28B data. At the time of the first auto-sample, breakthrough had already occurred at ports A, B and C. For ports D and E, it is possible to discern a ripening phase, but for the lower ports the noise drowns out the signal. After breakthrough, turbidity eventually stabilizes. Compared to the 28B data, the rising parts of the curves after breakthrough are slightly steeper in the Filtralite medium, but less steep in the sand medium, indicating slightly different dynamics of turbidity and virus removal in the two media. The mechanistic interpretation of such a pattern is not presently clear to us.

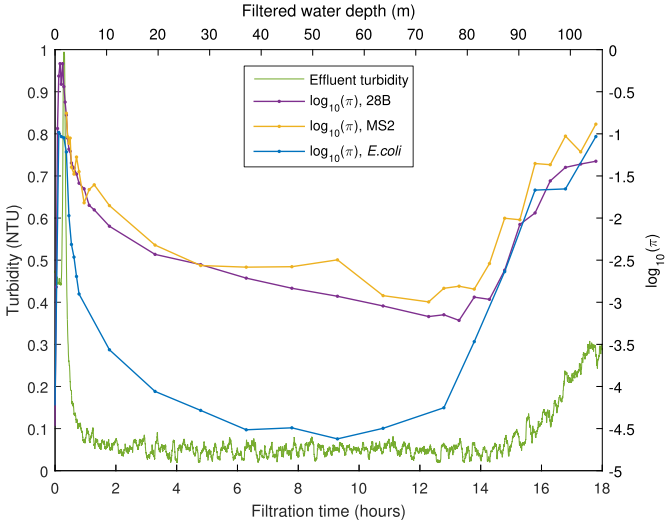

Fig. 3. Overall log-removal compared. Note that we discarded one suspicious data point for *E. coli* at approx 11. hours (comp. Fig. 2c), where we had two data points.

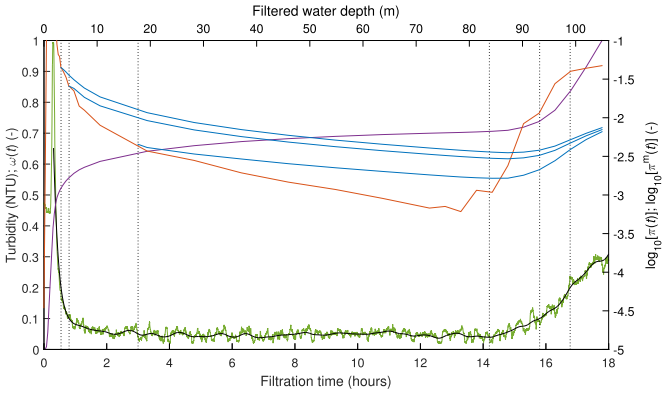

(a) Phage 28B mean removal evolution.

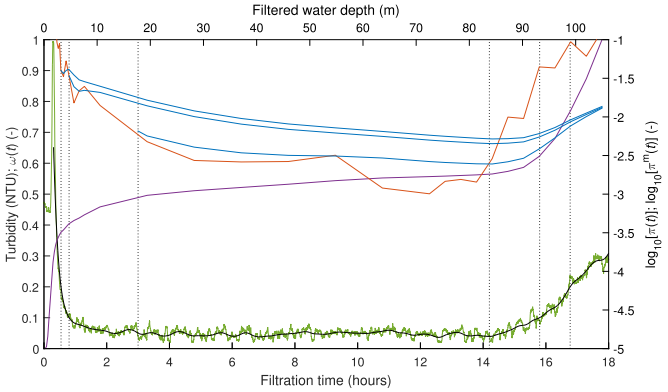

(b) Phage MS2 mean removal evolution, RT-qPCR data.

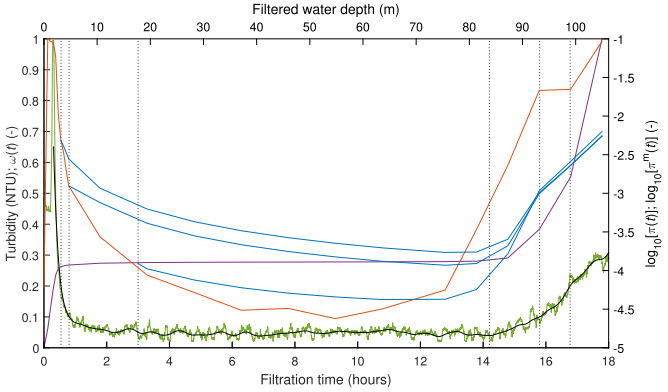

(c) *E. coli* mean removal evolution.

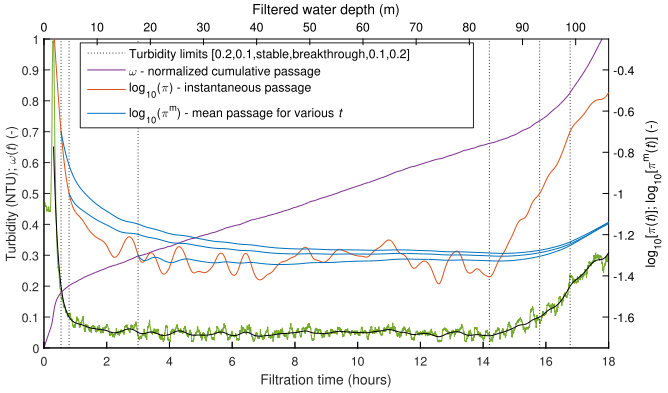

(d) Turbidity mean removal evolution, online measurements.

Fig. 4. Mean removal evolution of microorganisms and turbidity.

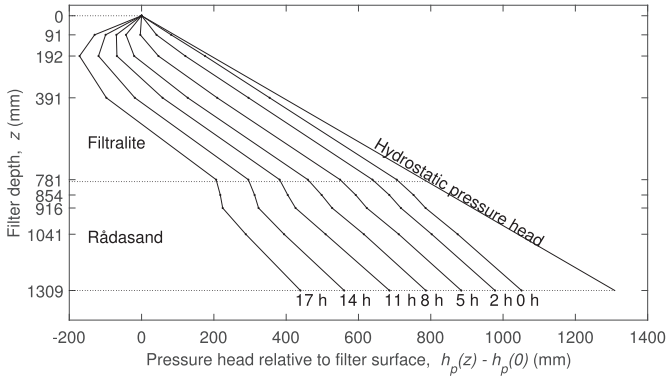

Fig. 5. Michau-diagram.

3.2.5. Removal compared

Fig. 3 shows the passage probability for all organisms in a single plot. The two viruses behave quite similarly while *E. coli* is both removed to a greater extent and shows faster ripening and earlier breakthrough than the viruses. These observations are qualitatively consistent with earlier observations on the ripening and breakthrough behavior of differently sized particles (Clark et al., 1992; Kim and Lawler, 2008; Moran et al., 1993), although it should be emphasized that a variety of factors besides particle size may play a role in the observed relationships, including (variations in) particle/floc and media surface geometry and surface charge, particle/floc density etc. The removal efficiencies of phages MS2 and 28B appear to be quite similar under these experimental conditions. These are both nearly spherical viruses, but 28B is about twice as large as MS2. Towards the very end of the cycle the removal efficiencies appear to converge. Although we have no firm explanation for this latter observation, one may speculate that removal mechanisms that are relatively independent of microorganism properties become more important at this stage.

Since zeta potential measurements are not available for this experiment, it is rather difficult to assess the influence of surface charge effects in controlling removal. The isoelectric points (IEP) of all three microorganisms are in the range 2–4 and they are therefore all negatively charged at the experimental pH, but that is all that can be said without zeta potential data. The IEP of MS2 is usually reported as between 3.1 and 3.9 (Michen and Graule, 2010), the IEP of 28B was reported recently as 3.8 (Christensen et al., 2017) and the IEP of *E. coli* appears to be between 2 and 3 (Lytle et al., 2002). The pattern with removal efficiencies for 28B ≈ MS2 < *E.coli* was also observed with zirconium (a four valent metal) and chitosan (a natural organic polymer) coagulants with similar raw water and optimized coagulation (Christensen et al., 2017).

3.2.6. Mean removal evolution

Perhaps the most interesting analysis made possible by the high-resolution data is the much refined computation of *mean* removal efficiency during the productive part of the filter cycle, and the *evolution* of this mean removal as the filter cycle progresses. Let t_1 be the time when the filter is put into operation after a backwash event (end of filter-to-waste). Then the mean probability of passage, π^m, during the time interval from t_1 to t is given by

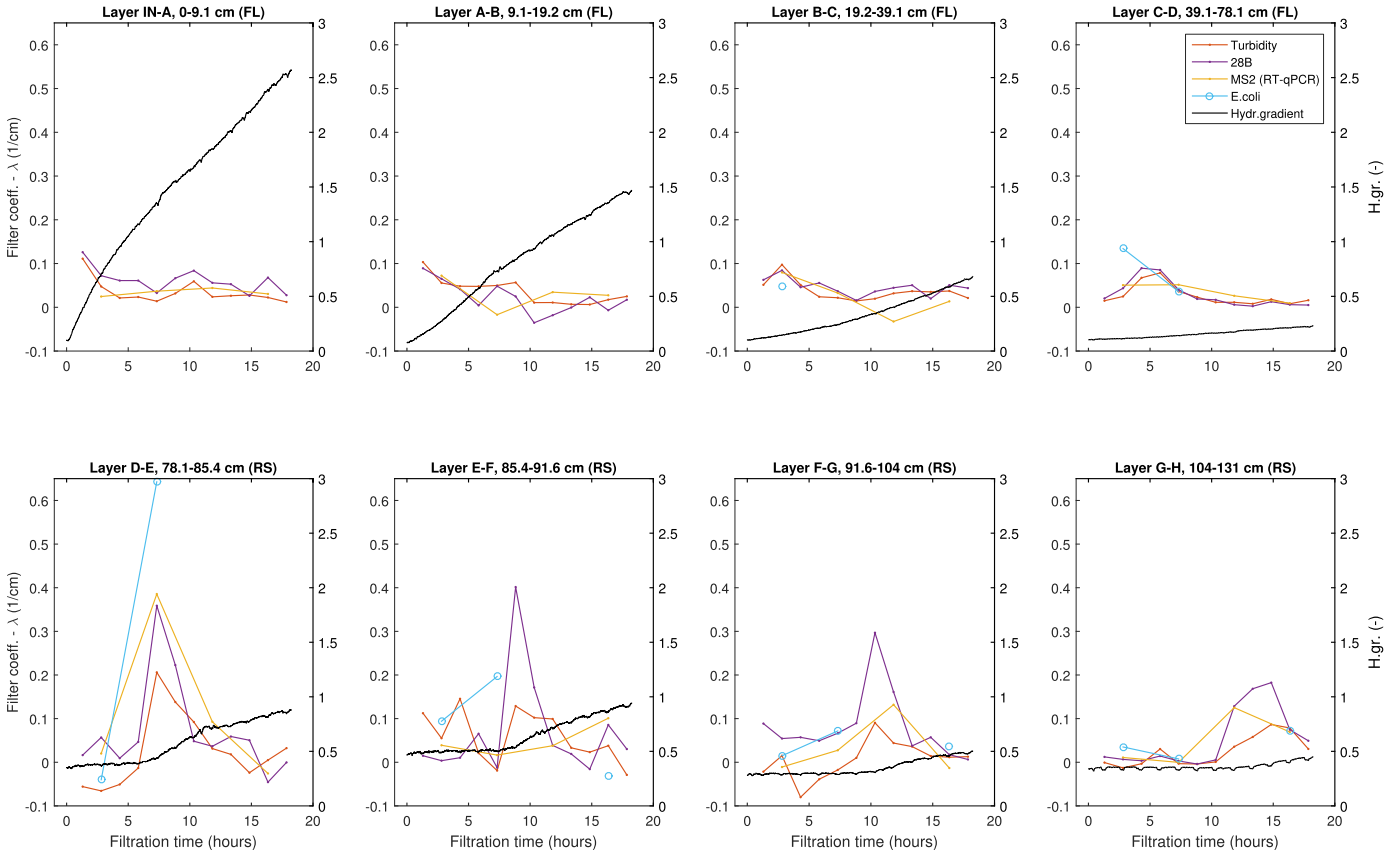

Fig. 6. Estimated filter coefficients from equation (8), and hydraulic gradients. Filter coefficients for *E. coli* could not be computed for several layers/times because samples were above the enumeration limit. FL - Filtralite; RS - Rådasand.

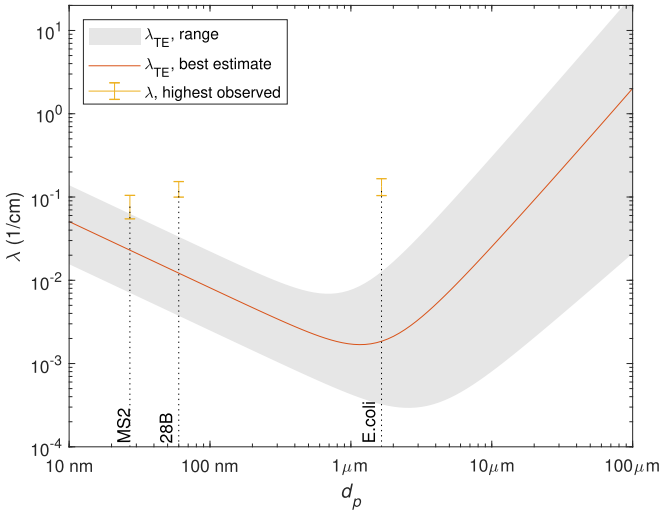

(a) Comparison for Filtralite. The grey area is the possible range of λ-values using the following parameters, with the parameters used for the best estimate in the middle: Porosity 0.48 – 0.58 – 0.63; Grain size 0.7 – 0.95 – 1.6 mm; Hamaker constant 1e-21 – 1e-20 – 1e-19 J; Density 1000 – 1250 – 2600 kg/m^3.

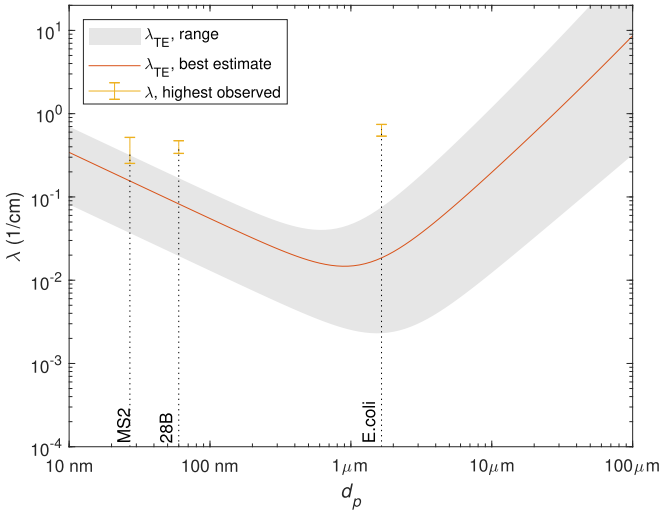

(b) Comparison for Rådasand. The grey area is the possible range of λ-values using the following parameters, with the parameters used for the best estimate in the middle: Porosity 0.35 – 0.45 – 0.50; Grain size 0.35 – 0.40 – 0.8 mm; Hamaker constant 1e-21 – 1e-20 – 1e-19 J; Density 1000 – 1250 – 2600 kg/m^3.

Fig. 7. Comparison of peak values of λ from Fig. 6 with those predicted by the TE correlation equation. All computations were carried out for water at 15°C.

$$\pi^{\mathrm{m}}(t) = \frac{\int_{t_1}^{t} q(\tau)c(\tau)\,\mathrm{d}\tau}{\int_{t_1}^{t} q(\tau)c_{\mathrm{in}}(\tau)\,\mathrm{d}\tau} \overset{q\ \mathrm{const.}}{=} \frac{\int_{t_1}^{t} c(\tau)\,\mathrm{d}\tau}{\int_{t_1}^{t} c_{\mathrm{in}}(\tau)\,\mathrm{d}\tau} \tag{2}$$

where q is the filtration rate (constant in our experiment). Using $\pi = c/c_{\mathrm{in}}$ and the fact that c_{in} was also constant in our experiment, we have

$$\pi^{\mathrm{m}}(t) = \frac{\int_{t_1}^{t} \pi(\tau)\,\mathrm{d}\tau}{t - t_1} \tag{3}$$

Assuming that $\pi(t)$ is differentiable, it is readily verified that potential minima of $\pi^{\mathrm{m}}(t)$ for $t > t_1$ occur when

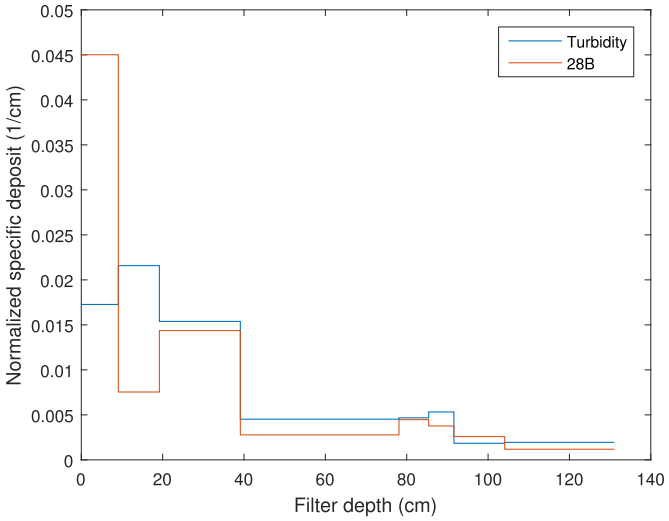

Fig. 8. Estimated specific deposit distribution at the end of the cycle. The vertical axis is normalized with respect to the total deposit so that the area under the curves are 1.

$$\pi^{\mathrm{m}}(t) = \pi(t) \tag{4}$$

which, for a typical U-shaped time evolution of $\pi(t)$ has a unique solution. Thus, if t_1 and $\pi(t)$ is given, termination of the filter run to minimize mean pathogen passage corresponds to ending the filter run at a time $t = t_2$ that solves (4). The online supplementary material discusses optimal filter runs if we let both t_1 and t_2 be free to choose.

This is illustrated in Fig. 4, which shows $\pi^{\mathrm{m}}(t)$ for viruses (4a and 4b) and bacteria (4c) for three values of t_1, corresponding to the events of turbidity falling below 0.2 and 0.1 NTU, and turbidity becoming stable (after approximately 3 h). Also shown is $\pi(t)$ and the normalized cumulative passage ω from our experimental data, defined as

$$\omega(t) = \frac{\int_0^{t} q(\tau)c(\tau)\,\mathrm{d}\tau}{\int_0^{t_{\mathrm{stop}}} q(\tau)c(\tau)\,\mathrm{d}\tau} \overset{q,\ c_{\mathrm{in}}\mathrm{const.}}{=} \frac{\int_0^{t} \pi(\tau)\,\mathrm{d}\tau}{\int_0^{t_{\mathrm{stop}}} \pi(\tau)\,\mathrm{d}\tau} \tag{5}$$

where t_{stop} is the end time of the experimental run. Thus, $\omega(t)$ gives the ratio of the number of microorganisms that has passed at time t to the total number of organisms that passed during the entire experimental run. The curves in Fig. 4 were computed by direct trapezoidal integration of experimental data.

There are several points to note in Fig. 4. First, the normalized cumulative passage curves $\omega(t)$ are quite different for viruses and bacteria. Approximately 40–50% of the virus passage happened in the early stages of the cycle before ripening brought effluent turbidity down to 0.2 NTU; the equivalent figure for bacteria is only about 25%.[2] After turbidity dropped below 0.2 NTU, $\omega(t)$ is quite flat for bacteria while it continues to flatten for viruses, reflecting different ripening behaviors. Consequently, most of the bacterial passage happened towards the end of the cycle.

Second, the marked difference between the instantaneous $\pi(t)$ and the mean $\pi^{\mathrm{m}}(t)$ is apparent. When starting water production at turbidity 0.2 NTU, the difference is about 1 log-unit at the time of

[2] Rough estimate since the peak in *E. coli* concentrations were missed because samples were above the enumeration limit (Fig. 2c).

microorganism breakthrough. It is also clear that $\pi^m(t)$ varies somewhat depending on when the filter-to-waste period is terminated, and the effect is particularly noticeable if one postpones the production start until turbidity is completely stable, at 3 h (usually not feasible). Once breakthrough has occurred, the different $\pi^m(t)$ curves start to converge. The overall mean log-removal between 32 min (turbidity dropped below 0.2 NTU) and 14.2 h (onset of turbidity breakthrough) was computed as 2.5, 2.3 and 3.6 for 28B, MS2 and *E. coli*, respectively. This is significantly lower than the corresponding peak log-removal of 3.2, 3.0 and 4.5, respectively, but higher than the log-credit values suggested by Ødegaard et al. (2014) (1.5/2.0 for viruses and 2.25/2.5 for bacteria). Hijnen and Medema (2010), in their review, reported much lower mean removal efficiencies, but their estimates included waste water studies and were also weighted strongly in favor of full-scale studies. The study that comes closest to our study in terms of raw water characteristics and experimental setup is the one by Hendricks et al. (2006) (indexed 38 and 39 in Tables S1 and S2), who reported a log-removal for MS2 of 2.9 (two-hour mean obtained mid-cycle). Huck et al. (2001) (indexed 34 in Tables S.1 and S.2) also observed an increase in log-removal efficiency for MS2 during end-of-run conditions before turbidity breakthrough (2.0 $\log_{10}$ units) compared to mid-cycle removal (1.4 $\log_{10}$ units). Their raw water was quite similar to the present study, but coagulant doses were lower and they used a cationic polymer. Interestingly, they observed much lower *E.coli* mid-cycle removal (about 0.5 $\log_{10}$ units) than the present study.

Third, it is interesting to compare the locations of minima in $\pi(t)$, i.e. time of conventional breakthrough, and minima in $\pi^m(t)$, i.e. the time of minimized organism passage. For viruses, breakthrough occurred slightly before turbidity breakthrough, but the minimum of $\pi^m(t)$ for viruses occurred *at* (MS2) or slightly *after* (28B) turbidity breakthrough, and 1–2 h after virus breakthrough. The location of the minimum of $\pi^m(t)$ for viruses does not depend strongly on t_1, the start of the production period, since the passage probability rises so quickly for viruses after breakthrough. For bacteria, the situation is different; the minima of both $\pi(t)$ and $\pi^m(t)$ occurred several hours *before* turbidity breakthrough. The exact location of the minimum of $\pi^m(t)$ is more sensitive to t_1 since the passage probability of bacteria rises more slowly in the time right after breakthrough. Continuing water production until turbidity reaches 0.2 NTU was clearly more detrimental to mean bacteria passage than mean virus passage in this case, since the overall increase in $\pi(t)$ for bacteria is greater than for viruses. It is clear that one cannot strictly optimize for mean bacteria and mean virus passage simultaneously for such a pattern, but ending the filter cycle at 13–14 h was close to optimal for all microorganisms investigated.

Fig. 4d shows identical computations performed for the turbidity data, with the caveat that concepts such as "proportion of turbidity passed" may not be entirely well-defined for turbidity, which is not a strictly conserved quantity. Nevertheless, the panel indicates that a greater proportion of the effluent turbidity passage occurred during the period of stable operation, i.e. less of the turbidity passage happened during ripening and breakthrough periods, as compared to the microorganisms. Furthermore, the minimum of $\pi^m(t)$ for turbidity occurred almost immediately after turbidity breakthrough, and practically at the same location as for viruses.

3.3. Headloss

Fig. 5 shows the Michau-diagram for the filter run, which confirms that most of the headloss increase occurred in the upper part of the Filtralite layer, but there was also some headloss development in the upper part of the sand layer.

4. Interpretations in terms of filtration modeling

Classical macroscopic filtration models that describe the dynamic behavior of the filtration process consist essentially of a particle volume conservation equation and a constitutive filtration rate equation (Iwasaki, 1937; Herzig et al., 1970; Tien and Ramaro, 2007), respectively:

$$\frac{\partial \sigma}{\partial t} + u\frac{\partial c}{\partial z} = 0 \tag{6}$$

$$\frac{\partial c}{\partial z} = -\lambda c \tag{7}$$

Here c is the suspended particle concentration (volume of particles per unit volume of suspension, dim.less), σ is the specific deposit (volume of particles per unit volume of porous medium, dim.less), u is the Darcy velocity (L/T) and λ is the filter coefficient (1/L). The former equation assumes that dispersive transport is negligible as well as other simplifying approximations (Horner et al., 1986). The latter was first proposed by Iwasaki (1937) and remains a standard assumption. The system above does not consider particle detachment, which may be a limitation.

The main challenge in deep bed filtration is that λ changes with time as the filter collects particles and it also changes with depth in the filter. Thus, λ is usually taken as a function of σ, and is called the *filtration function*. Work is ongoing to investigate if there exist appropriate filtration functions for this dataset. In the following, we rely directly on the data rather than simulation results.

4.1. Experimental filter coefficients

Here, crude estimates of the mean filter coefficient in each layer were determined directly from the experimental data by computing

$$\lambda_{i,i+1} = \frac{1}{z_{i+1} - z_i}\ln\left(\frac{c_i}{c_{i+1}}\right) \tag{8}$$

where c_i is the concentration/turbidity in port i and c_{i+1} is the concentration in the nearest port below, both at a given time.

Fig. 6 shows the results along with the hydraulic gradients for each layer. The data are noisy since we are essentially estimating derivatives based on two data points that are both a little noisy, but the wave-like progression across the filter depth of the peak in λ can clearly be seen. The highest filter coefficients occurred in the upper part of the sand layer (which was partly mixed with Filtralite after backwashing). Note the lower temporal sampling resolution of the MS2/*E. coli* data, which masks some of their dynamics. Note also that the distance between sample ports varied so that one may expect that some peaks are "averaged down" as one moves to the rightmost panels in Fig. 6. The hydraulic gradient in the lower part of the sand layer started to rise after about 12 h, thereby giving an "early" warning that turbidity breakthrough was imminent. The gradient increased some 30-fold in the upper part of the Filtralite, and there is a variation in initial hydraulic gradients between the various sand layers, another indication that there was some mixing of sand and Filtralite.

4.2. Comparison with ideal filtration theory

The filter coefficients in Fig. 6 may be compared to those estimated from ideal filtration theory, assuming that near steady-state

conditions prevail during each 10-min sampling interval. Substantial research has been devoted to estimating λ from first-principles and has been largely successful under favorable conditions for filtration, i.e. no repulsive electrostatic interactions between particles and filter grains (Tufenkji, 2007). In this theory, the filter coefficient is given by:

$$\lambda = \frac{3}{2}\frac{(1-\varepsilon)}{d_c}\alpha\eta_0 \quad (9)$$

Here ε is the porosity, d_c is the filter grain (collector) diameter, η_0 is the so-called single-collector contact efficiency and α the sticking efficiency. The latter is assumed to be 1 under favorable conditions. The currently most widely used equation for estimating η_0 was developed by Tufenkji and Elimelech (2004).

Fig. 7 compares peak values of λ taken from Fig. 6 with those predicted by equation (9), using the expression for η_0 from Tufenkji and Elimelech (2004). The uncertainty intervals for observed λ-values were computed using 95% confidence intervals for concentrations, see Figures S.6 - S.8 in the online supplementary material. In equation (9), α was taken as 1, assuming that sufficient coagulation and ripening for favorable conditions had occurred at the time of peak removal. For size-graded porous media, as our filter media, it has been recommended to compute η_0 and λ using a grain size that emphasizes the smaller grain fractions, such as d_{10} (Pazmino et al., 2011), hence we followed this recommendation. In order to account for uncertainty in the input parameters to the calculation of η_0, the grey bands in Fig. 7 show a range of λ-values corresponding to a very wide range in the input parameter values assumed to cover all plausible values applicable to our experiment (see the figure caption), even accounting for the effect of the already retained particles (O'Melia and Ali, 1979).

From Fig. 7, it is seen that the observed peak λ-values are outside the grey bands except for MS2 (barely), indicating that observed peak λ-values were largely inconsistent with those computed from colloid filtration theory based on known microorganism sizes. Thus, even assuming perfectly favorable filtration conditions ($\alpha = 1$) and allowing for a wide range of input parameters, peak observed removal were higher than predicted by filtration theory. Possible explanations include departures from the ideal assumptions of filtration theory (e.g. the effect of the pore space being partly filled with deposit) and microorganism-floc association.

4.3. Deposit distribution at end-of-cycle

Fig. 8 shows the results of a simple numerical (trapezoidal) integration of equation (6) directly from the experimental data for c, and indicates how the deposit of particles (c for particles assumed proportional to turbidity) and 28B was distributed in the filter column at the end of the experiment. Most of the deposit is in the upper part of the Filtralite for both particles and 28B, but there is also a noticeable accumulation of deposit in the upper part of the sand layer. There is also some non-monotonicity within each filter medium.

5. Overall discussion

Our results were obtained in a single filter run under a single set of conditions and, as such, generalizations from our computed removal efficiencies should be done with care. The filtration performance may be affected by a range of factors such as e.g. raw water quality, coagulant type and dose, use of filter aids, filtration rate, backwash strategies etc. (Hijnen and Medema, 2010). In particular, our raw water was relatively high in NOM and low in turbidity whereas in many places the opposite situation with low NOM and high turbidity is more common. High NOM and low turbidity usually requires higher coagulant doses and stricter pH control (Edzwald and Tobiason, 1999). There was no direct confirmation by e.g. zeta potential measurements that coagulation conditions were optimal in our experiment. As mentioned in the introduction, effective filtration depends on adequate coagulation. For parasites, it has been demonstrated that removal may be sensitive to suboptimal coagulation conditions (Huck et al., 2001, 2002). Still, this study demonstrates how dynamic the filter performance may be for viruses and bacteria, and what analyses can be performed when high-resolution data is available. The dynamic microorganism removal observed in this study, even during the period of stable effluent turbidity, signals that care should be taken when characterizing microbial removal efficiencies during filtration. Either samples should be taken frequently, such as in this study, or at least flow-proportional continuous sampling should be employed to better estimate true mean removal efficiencies.

The usefulness of surrogates, such as phages, for studying removal and inactivation of pathogenic viruses is a continuous concern (Mesquita and Emelko, 2012; Sinclair et al., 2012). Recent research (Shi and Tarabara, 2018) also suggests that laboratory preparation methods (propagation, purification) for viruses may affect their charge and size distributions as well as hydrophobicity. Hijnen and Medema (2010) suggested that coliphages are appropriate surrogates for pathogenic viruses in deep bed filtration. Since *Salmonella* typhimurium phage 28B is simple to work with, it would be a useful addition to the set of surrogate phages if it can be confirmed that it behaves similarly to MS2 and/or other coliphages under a wide range of conditions. We believe this study and Christensen et al. (2017) are the first to use this phage for deep bed filtration experiments for drinking water. Examples of previous applications include waste water transport in soils (Carlander et al., 2000), small-scale waste water treatment systems (Heistad et al., 2009a, b) and biofilter performance in drinking water treatment (Persson et al., 2005).

A concern regarding the applicability of these results, and those from most other pilot-scale studies, is the high influent concentrations used for the microorganisms; much higher than what occurs naturally. Assavasilavasukul et al. (2008) observed better removal of *Cryptosporidium* during conventional treatment with higher *Cryptosporidium* influent concentrations. Prasanthi et al. (1997) also observed better removal with higher influent concentrations in laboratory columns without coagulation. However, it is not clear whether these results apply to viruses in our experiment. The virus volume is negligible compared to the total floc volume, virus aggregation was not detected, and according to standard flocculation theory the virus-floc aggregation rate is expected to scale linearly with virus concentrations and thus variations in virus concentrations shouldn't affect removal efficiencies. Further research is needed to clarify these issues. Finally, the role of virus detachment is also not clear (Kim and Tobiason, 2004). If virus detachment is not negligible compared to virus attachment, the number of viruses available for detachment becomes important and therefore the observed removal efficiencies may become a function of the influent concentrations.

The concentrations of all three microorganisms in the influent were chosen sufficiently high that there was no need for dedicated concentration steps during enumeration, even for effluent samples taken during peak removal. Issues associated with analytical recoveries were therefore largely avoided, although there may still have been some losses to glassware and plastics (pipettes, tubes) used in the lab. These losses are, however, difficult to assess. Since all the removal efficiencies are calculated from the ratio of two concentrations, losses that are proportional to concentrations would not affect these removal values (except for added noise).

6. Conclusions

The following conclusions may be drawn from this work:

1. Both virus and *E. coli* filtration performance was dynamic, showing variations in removal efficiencies during periods of stable effluent turbidity.
   - Ripening and breakthrough for *E. coli* occurred earlier than for viruses. Both deviated from turbidity.
   - Regulatory limits on turbidity (typically less than 0.2 NTU) appear not to ensure stable operation with respect to virus/*E. coli* removal.
2. True mean log-removal estimates over complete cycles of water production deviated significantly from instantaneous log-removal values.
   - Careful design of sampling regimes is needed to correctly estimate mean removal efficiencies in filtration experiments.
   - Reporting the removal efficiency of a deep bed filter with a single number may be inappropriate, unless the single number is a properly computed mean removal efficiency.
3. Peak removal of viruses and bacteria between adjacent sampling ports were higher than computed with ideal filtration theory.
4. More high-resolution studies of microbial filtration performance should be performed in order to collect data under a wider range of conditions.
   - We recommend that future studies present results in a manner similar to Fig. 4, with an axis for total filtered water depth to facilitate comparison between different filter and operational configurations.

We emphasize again that the main purpose of this study was to generate a high-resolution (both in space and time) mapping of the removal performance throughout a filter cycle, mainly with respect to viruses. To our knowledge, this is the first such high-resolution mapping. While it would have been desirable to have multiple runs to assess variability between runs and experimental conditions, this is a very resource-intensive type of investigation, which meant that we only saw it possible to run one cycle. The main result is that we could demonstrate the impact of time variation on the calculation of mean removal efficiencies. While the pattern of time variation may vary between settings or even with aging, we believe our study demonstrates the importance of capturing it and accounting for it.

Declaration of interests

The authors declare that they have no known competing financial interests or personal relationships that could have appeared to influence the work reported in this paper.

Conflicts of interest

No conflict of interest declared.

Acknowledgements

E. Christensen acknowledges the financial support from the Research Council of Norway (grant no. 226750/O30) and Norconsult AS consultancy firm. The authors would like to thank Arne Svendsen and Tom Ringstad for their invaluable role in designing and constructing the filtration column and automatic sampler. Anne Willumsen, MSc, and Torbjørn Friborg, MSc, provided much-needed assistance with the 28B analyses. Thanks also go to Jon Fredrik Hanssen, Else Aasen and Rannei Tjåland for assisting with microbiology laboratory preparations. The water treatment plant at Nedre Romerike Vannverk provided practical assistance with raw water for these experiments and helped finance the transport of raw water from the plant to the university. Tor Håkonsen, PhD, and Prof. Lars Hem provided advice on various aspects of the design and operation of the filtration system.

Appendix A. Supplementary data

Supplementary data to this article can be found online at https://doi.org/10.1016/j.watres.2019.02.029.

References

Adin, A., Rebhun, M., 1974. High-rate contact flocculation–filtration with cationic polyelectrolytes. J. Am. Water Work. Assoc. 66, 109–117.
Amirtharajah, A., 1988. Some theoretical and conceptual views of filtration. J. Am. Water Work. Assoc. 80, 36–46.
APHA/AWWA/WEF, 2012. Standard Methods for the Examination of Water and Wastewater, 22 ed. American Public Health Association, American Water Works Association, Water Environment Federation.
Assavasilavasukul, P., Lau, B.L.T., Harrington, G.W., Hoffman, R.M., Borchardt, M.A., 2008. Effect of pathogen concentrations on removal of *Cryptosporidium* and *giardia* by conventional drinking water treatment. Water Res. 42, 2678–2690. https://doi.org/10.1016/j.watres.2008.01.021.
Carlander, A., Aronsson, P., Allestam, G., Stenström, T.A., Perttu, K., 2000. Transport and retention of bacteriophages in two types of willow-cropped lysimeters. J. Environ. Sci. Health - Part A Toxic/Hazard. Subst. Environ. Eng. 35, 1477–1492. https://doi.org/10.1080/10934520009377048.
Christensen, E., Myrmel, M., 2018. Coagulant residues' influence on virus enumeration as shown in a study on virus removal using aluminium, zirconium and chitosan. J. Water Health 16, 600–613. https://doi.org/10.2166/wh.2018.028.
Christensen, E., Nilsen, V., Håkonsen, T., Heistad, A., Gantzer, C., Robertson, L.J., Myrmel, M., 2017. Removal of model viruses, *E.coli* and *Cryptosporidium* oocysts from surface water by zirconium and chitosan coagulants. J. Water Health 15, 695–705. https://doi.org/10.2166/wh.2017.055.
Clark, S.C., Lawler, D.F., Cushing, R.S., 1992. Contact filtration: particle size and ripening. J. Am. Water Work. Assoc. 84, 61–71.
Debartolomeis, J., Cabelli, V.J., 1991. Evaluation of an escherichia-coli host strain for enumeration of F-Male-Specific bacteriophages. Appl. Environ. Microbiol. 57, 1301–1305.
Dreier, J., Stormer, M., Kleesiek, K., 2005. Use of bacteriophage MS2 as an internal control in viral reverse transcription-PCR assays. J. Clin. Microbiol. 43, 4551–4557. https://doi.org/10.1128/JCM.43.9.4551-4557.2005.
Edberg, S.C., Rice, E.W., Karlin, R.J., Allen, M.J., 2000. *Escherichia coli*: the best biological drinking water indicator for public health protection. J. Appl. Microbiol. 88, 106S–116S. https://doi.org/10.1111/j.1365-2672.2000.tb05338.x.
Edzwald, J.K., Tobiason, J.E., 1999. Enhanced coagulation: US requirements and a broader view. Water Sci. Technol. 40, 63–70. https://doi.org/10.1016/S0273-1223(99)00641-1.
Eikebrokk, B., 2012. Veiledning for drift av koaguleringsanlegg. Technical Report. Norsk Vann. Report number 188-2012 (in Norwegian).
Eikebrokk, B., Saltnes, T., 2001. Removal of natural organic matter (NOM) using different coagulants and lightweight expanded clay aggregate filters. Water Sci. Technol. Water Supply 1, 131–140.
Eikebrokk, B., Vogt, R.D., Liltved, H., 2004. NOM increase in northern european source waters: impacts on coagulation/contact filtration processes. In: Newcombe, G., Ho, L. (Eds.), Natural Organic Material Research: Innovations and Applications for Drinking Water (Selected Papers of the 3rd International Conference on Natural Organic Material Research: Innovations and Applications for Drinking Water, Held in Victor Harbor, South Aus. IWA Publishing.
Haas, C.N., Rose, J.B., Gerba, C.P., 2014. Quantitative Microbial Risk Assessment, 2 ed. John Wiley & Sons, Inc, Hoboken, New Jersey. https://doi.org/10.1002/9781118910030.
Harrington, G.W., Xagoraraki, I., Assavasilavasukul, P., Standridge, J.H., 2003. Effect of filtration conditions on removal of emerging pathogens. J. Am. Water Work. Assoc. 95, 95–104.
Heistad, A., Scott, T., Skaarer, A.M., Seidu, R., Hanssen, J.F., Stenström, T.A., 2009a. Virus removal by unsaturated wastewater filtration: effects of biofilm accumulation and hydrophobicity. Water Sci. Technol. 60, 399–407. https://doi.org/10.2166/wst.2009.343.
Heistad, A., Seidu, R., Fløe, A., Paruch, A.M., Hanssen, J.F., Stenström, T.A., 2009b. Long-term hygienic barrier efficiency of a compact on-site wastewater treatment system. J. Environ. Qual. 38, 2182–2188. https://doi.org/10.2134/jeq2008.0407.
Hellemans, J., Mortier, G., De Paepe, A., Speleman, F., Vandesompele, J., 2007. qBase relative quantification framework and software for management and automated analysis of real-time quantitative PCR data. Genome Biol. 8, R19. https://doi.org/10.1186/gb-2007-8-2-r19.
Hendricks, D.W., Clunie, W.F., Sturbaum, G.D., Klein, D.A., Champlin, T.L., Kugrens, P.,

Hirsch, J., Mccourt, B., Nordby, G.R., Sobsey, M.D., Hunt, D.J., Allen, M.J., 2006. Filtration removals of microorganisms and particles. J. Environ. Eng. 131, 1621–1632. https://doi.org/10.1061/(ASCE)0733-9372(2005)131:12(1621).

Herzig, J.P., Leclerc, D.M., Le Goff, P., 1970. Flow of suspensions through porous Mediaâ€" application to deep filtration. Ind. Eng. Chem. 62, 8–35. https://doi.org/10.1021/ie50725a003.

Hijnen, W.A.M., Medema, G.J., 2010. Elimination of Microorganisms by Water Treatment Processes. IWA Publishing. https://doi.org/10.2166/9781780401584.

Höglund, C., Ashbolt, N., Stenström, T.A., Svensson, L., 2002. Viral persistence in source-separated human urine. Adv. Environ. Res. 6, 265–275. https://doi.org/10.1016/S1093-0191(01)00057-0.

Horner, R.M.W., Jarvis, R.J., Mackie, R.I., 1986. Deep bed filtration: a new look at the basic equations. Water Res. 20, 215–220. https://doi.org/10.1016/0043-1354(86)90011-4.

Huck, P.M., Coffey, B.M., Emelko, M.B., Maurizio, D.D., Slawson, R.M., Anderson, W.B., van den Oever, J., Douglas, I.P., O'Melia, C.R., 2002. Effects of filter operation on Cryptosporidium removal. J. Am. Water Work. Assoc. 94, 97–111.

Huck, P.M., Emelko, M.B., Coffee, B.M., Maurizio, D.D., O'Melia, C.R., 2001. Filter Operation Effects on Pathogen Passage. AWWA Research Foundation.

ISO, 1995. ISO 10705-1:1995. Water Quality - Detection and Enumeration of Bacteriophages - Part 1: Enumeration of F-specific RNA Bacteriophages. Technical Report. International Standards Organization.

ISO, 1999. ISO10705-2:2000. Water Quality - Detection and Enumeration of Bacteriophages - Part 2: Enumeration of Somatic Coliphages. Technical Report. International Standards Organization.

Iwasaki, T., 1937. Some notes on sand filtration. J. Am. Water Work. Assoc. 29, 1591–1602.

Keswick, B.H., Gerba, C.P., DuPont, H.L., Rose, J.B., 1984. Detection of enteric viruses in treated drinking water. Appl. Environ. Microbiol. 47, 1290–1294.

Kim, J., Lawler, D.F., 2008. Influence of particle characteristics on filter ripening. Separ. Sci. Technol. 43, 1583–1594. https://doi.org/10.1080/01496390801974688.

Kim, J., Tobiason, J.E., 2004. Particles in filter effluent: the roles of deposition and detachment. Environ. Sci. Technol. 38, 6132–6138. https://doi.org/10.1021/es0352698.

Kreißel, K., Bösl, M., Hügler, M., Lipp, P., Franzreb, M., Hambsch, B., 2014. Inactivation of F-specific bacteriophages during flocculation with polyaluminum chloride â€" a mechanistic study. Water Res. 51, 144–151. https://doi.org/10.1016/j.watres.2013.12.026.

Lang, J.S., Giron, J.J., Hansen, A.T., Trussell, R.R., Hodges Jr., W.E., 1993. Investigating filter performance as a function of the ratio of filter size to media size. J. Am. Water Work. Assoc. 85, 122–130.

Lilleengen, K., 1948. Typing of *Salmonella* Typhimurium by Means of Bacteriophage: an Experimental Bacteriologic Study for the Purpose of Devising a Phage-Typing Method to Be Used as an Aid in Epidemiologic and Epizootologic Investigations in Outbreaks of Typhimurium Inf (Phd. Royal Veterinary College, Stockholm).

Lytle, D.A., Johnson, C.H., Rice, E.W., 2002. A systematic comparison of the electrokinetic properties of environmentally important microorganisms in water. Colloids Surfaces B Biointerfaces 24, 91–101. https://doi.org/10.1016/S0927-7765(01)00219-3.

Mac Kenzie, W.R., Hoxie, N.J., Proctor, M.E., Gradus, M.S., Blair, K.A., Peterson, D.E., Kazmierczak, J.J., Addiss, D.G., Fox, K.R., Rose, J.B., Davis, J.P., 1994. A massive outbreak in milwaukee of *Cryptosporidium* infection transmitted through the public water supply. N. Engl. J. Med. 331, 161–167. https://doi.org/10.1056/NEJM199407213310304.

Matilainen, A., Vepsäläinen, M., Sillanpää, M., 2010. Natural organic matter removal by coagulation during drinking water treatment: a review. Adv. Colloid Interface Sci. 159, 189–197. https://doi.org/10.1016/j.cis.2010.06.007.

Matsui, Y., Matsushita, T., Sakuma, S., Gojo, T., Mamiya, T., Suzuoki, H., Inoue, T., 2003. Virus inactivation in aluminum and polyaluminum coagulation. Environ. Sci. Technol. 37, 5175–5180. https://doi.org/10.1021/es0343003.

Matsushita, T., Matsui, Y., Inoue, T., 2004. Irreversible and reversible adhesion between virus particles and hydrolyzing-precipitating aluminium: a function of coagulation. Water Sci. Technol. 50, 201–206.

Matsushita, T., Shirasaki, N., Matsui, Y., Ohno, K., 2011. Virus inactivation during coagulation with aluminum coagulants. Chemosphere 85, 571–576. https://doi.org/10.1016/j.chemosphere.2011.06.083.

Mehta, D., Hawley, M.C., 1969. Wall effect in packed columns. Ind. Eng. Chem. Process Des. Dev. 8, 280–282. https://doi.org/10.1021/i260030a021.

Mesquita, M.M.F., Emelko, M.B., 2012. Bacteriophages as surrogates for the fate and transport of pathogens in source water and in drinking water treatment processes. In: Kurtboke, I. (Ed.), Bacteriophages. InTech, pp. 57–80. https://doi.org/10.5772/34024 (chapter 4).

Michen, B., Graule, T., 2010. Isoelectric points of viruses. J. Appl. Microbiol. 109, 388–397. https://doi.org/10.1111/j.1365-2672.2010.04663.x.

Moran, D.C., Moran, M.C., Cushing, R.S., Lawler, D.F., 1993. Particle behavior in deep-bed filtration: Part 1â€"Ripening and breakthrough. J. Am. Water Work. Assoc. 85, 69–81.

Nygård, K., Wahl, E., Krogh, T., Tveit, O.A., Bøhleng, E., Tverdal, A., Aavitsland, P., 2007. Breaks and maintenance work in the water distribution systems and gastrointestinal illness: a cohort study. Int. J. Epidemiol. 36, 873–880. https://doi.org/10.1093/ije/dym029.

O'Melia, C.R., Ali, W., 1979. The role of retained particles in deep bed filtration. In: Jenkins, S. (Ed.), Water Pollution Research. Proceedings of the 9th International Conference. Pergamon Press, Stockholm, Sweden, pp. 167–182. https://doi.org/10.1016/B978-0-08-022939-3.50019-2, 1978.

Payment, P., Armon, R., 1989. Virus removal by drinking water treatment processes. Crit. Rev. Environ. Contr. 19, 15–31. https://doi.org/10.1080/10643389809388357.

Pazmino, E.F., Ma, H., Johnson, W.P., 2011. Applicability of colloid filtration theory in size-distributed, reduced porosity, granular media in the absence of energy barriers. Environ. Sci. Technol. 45, 10401–10407. https://doi.org/10.1021/es202203m.

Persson, F., Långmark, J., Heinicke, G., Hedberg, T., Tobiason, J., Stenström, T.A., Hermansson, M., 2005. Characterisation of the behaviour of particles in biofilters for pre-treatment of drinking water. Water Res. 39, 3791–3800. https://doi.org/10.1016/j.watres.2005.07.007.

Petterson, S.R., Ashbolt, N.J., 2016. QMRA and water safety management: review of application in drinking water systems. J. Water Health 14, 571–589. https://doi.org/10.2166/wh.2016.262.

Prasanthi, H., Vigneswaran, S., Dharmappa, H.B., 1997. Effect of particle concentration on the entire cycle of filtration. Water Sci. Technol. 35, 91–102. https://doi.org/10.1016/S0273-1223(97)00155-8.

Robeck, G.G., Clark, N.A., Dostal, K.A., 1962. Effectiveness of water treatment processes in virus removal. J. Am. Water Work. Assoc. 54, 1275–1292.

Rose, J.B., Gerba, C.P., Singh, S.N., Toranzos, G.A., Keswick, B., 1986. Isolating viruses from finished water. J. Am. Water Work. Assoc. 78, 56–61.

Sahlström, L., Bagge, E., Emmoth, E., Holmqvist, A., Danielsson-Tham, M.L., Albihn, A., 2008. A laboratory study of survival of selected microorganisms after heat treatment of biowaste used in biogas plants. Bioresour. Technol. 99, 7859–7865. https://doi.org/10.1016/j.biortech.2007.09.071.

Shi, H., Tarabara, V.V., 2018. Charge, size distribution and hydrophobicity of viruses: effect of propagation and purification methods. J. Virol Methods 256, 123–132. https://doi.org/10.1016/j.jviromet.2018.02.008.

Sinclair, R.G., Rose, J.B., Hashsham, S.A., Gerba, C.P., Haas, C.N., 2012. Criteria for selection of surrogates used to study the fate and control of pathogens in the environment. Appl. Environ. Microbiol. 78, 1969–1977. https://doi.org/10.1128/AEM.06582-11.

Strauss Jr., J.H., Sinsheimer, R.L., 1963. Purification and properties of bacteriophage MS2 and of its ribonucleic acid. J. Mol. Biol. 7, 43–54. https://doi.org/10.1016/S0022-2836(63)80017-0.

Svenson, S.B., Lönngren, J., Carlin, N., Lindberg, A.A., 1979. *Salmonella* bacteriophage glycanases: endorhamnosidases of *Salmonella typhimurium* bacteriophages. J. Virol. 32, 583–592.

Templeton, M.R., Andrews, R.C., Hofmann, R., 2007. Removal of particle-associated bacteriophages by dual-media filtration at different filter cycle stages and impacts on subsequent UV disinfection. Water Res. 41, 2393–2406. https://doi.org/10.1016/j.watres.2007.02.047.

Thurston-Enriquez, J.a., Haas, C.N., Jacangelo, J., Gerba, C.P., 2003. Chlorine inactivation of adenovirus type 40 and feline calicivirus. Appl. Environ. Microbiol. 69, 3979–3985. https://doi.org/10.1128/AEM.69.7.3979.

Tien, C., Ramaro, B.V., 2007. Granular Filtration of Aerosols and Hydrosols, 2 ed. Butterworth-Heinemann.

Tufenkji, N., 2007. Modeling microbial transport in porous media: traditional approaches and recent developments. Adv. Water Resour. 30, 1455–1469. https://doi.org/10.1016/j.advwatres.2006.05.014.

Tufenkji, N., Elimelech, M., 2004. Correlation equation for predicting single-collector efficiency in physiochemical filtration in saturated porous media. Environ. Sci. Technol. 38, 529–536. https://doi.org/10.1021/es034049r.

USEPA, 2006. National primary drinking water regulations: long term 2 enhanced surface water treatment Rule. Fed. Regist. 71, 654–786.

WHO, 2011. Guidelines for Drinking-Water Quality, 4 ed. World Health Organization, Geneva, Switzerland.

Willumsen, A., 2015. Undersøkelse av virusfjerning i modning- og gjennombruddsperiodene i et pilotskala to-media sandfilter for drikkevann [Pilot-Scale Investigations of Virus Removal During the Ripening and Breakthrough Phases in a Dual-Media Sand Filter for Drinking Water]. Msc. Norwegian University of Life Sciences.

Ødegaard, H., Eikebrokk, B., Storhaug, R., 1999. Processes for the removal of humic substances from water - an overview based on Norwegian experiences. Water Sci. Technol. 40, 37–46. https://doi.org/10.1016/S0273-1223(99)00638-1.

Ødegaard, H., Østerhus, S., Melin, E., Eikebrokk, B., 2010. NOM removal Technologies â€" Norwegian experiences. Drink. Water Eng. Sci. 3, 1–9. https://doi.org/10.5194/dwes-3-1-2010.

Ødegaard, H., Østerhus, S.W., Pott, B.M., 2014. Microbial barrier analysis (MBA) - a guideline. Technical report. Norsk Vann. Report number 202 - 2014.